Journal of Artificial Intelligence and Data Mining (JAIDM), Vol. 10, No. 1, 2022, 53-61.

Shahrood University of Technology

Journal of Artificial Intelligence and Data Mining (JAIDM)
Journal homepage: http://jad.shahroodut.ac.ir

Research paper

Automatic Shadow Direction Determination using Shadow Low Gradient Direction Feature in RGB VHR Remote Sensing Images

Mohammad Kakooei and Yasser Baleghi*

Electrical & Computer Engineering Department, Babol Noshirvani University of Technology, Babol, Iran.

Article Info

Article History:
Received 10 April 2021
Revised 05 September 2021
Accepted 13 December 2021

DOI:10.22044/JADM.2021.10705.2205

Keywords:
Shadow Direction, Feature Extraction, Shadow Detection, VHR, Google Earth Engine

**Corresponding author:*
y.baleghi@nit.ac.ir (Y. Baleghi).

Abstract

Shadow detection provides worthwhile information for remote sensing applications, e.g. building height estimation. Shadow areas are formed in the opposite side of the sunlight radiation to tall objects, and thus solar illumination angle is required to find probable shadow areas. In the recent years, Very High Resolution (VHR) imagery provides more detailed data from the objects including shadow areas. In this regard, the motivation of this paper is to propose a reliable feature, Shadow Low Gradient Direction (SLGD), to automatically determine shadow and solar illumination direction in the VHR data. The proposed feature is based on the inherent spatial feature of fine-resolution shadow areas. Therefore, it can facilitate shadow-based operations, especially when the solar illumination information is not available in remote sensing metadata. Shadow intensity is supposed to be dependent on two factors including the surface material and sunlight illumination, which is analyzed by directional gradient values in low gradient magnitude areas. This feature considers the sunlight illumination, and ignores the material differences. The method is fully implemented on the Google Earth Engine cloud computing platform, and is evaluated on the VHR data with 0.3 m resolution. Finally, the SLGD performance is evaluated in determining shadow direction and compared in refining shadow maps.

1. Introduction

Shadow area analysis is an active research topic in Very High resolution (VHR) optical Remote Sensing (RS) [1]. In this regard, RS, optical, and VHR are three important key points in the current research works. Firstly, RS includes all instruments that remotely acquire data from the earth surface including satellite, airborne, and Unmanned Aerial Vehicle (UAV) imagery platforms [2]. Secondly, optical RS imagery, which is passive and is dependent on the sunlight radiation backscattering, provides such an object representation that is similar to human vision, and thus is popular in an object-based analysis [3]. On the other hand, shadow analysis is just meaning-full in optical RS, in which shadow area is formed where the sunlight radiation does not directly reach the ground [4]. It means that the shadow is the clue of the existing tall object on the ground surface [5]. In this regard, detection of tall objects such as buildings and trees is interested in many applications, especially in the urban areas [6, 7]. Thirdly, using VHR images, in which fine object analysis becomes possible, is becoming more and more accessible due to the continuous development of RS technology in the recent years [3, 8, 9]. It is also expected to extract more informative features from the shadow areas, and deploy it to develop more accurate models [10]. Therefore, in this work, we proposed a new shadow feature in the optical VHR RS data.

The shadow detection methods are divided into two categories including model-based and feature-

based methods. The model-based methods are more accurate than the feature-based ones but they require extra information such as solar azimuth. On the other hand, the feature-based methods are more straight, and just utilize the image processing techniques in order to find the shadow area [11]. Furthermore, the feature-based methods are more practical in the real-world applications [12]. Therefore, in order to increase the accuracy of the feature-based methods and make them more reliable in the real-world applications, we proposed a feature to automatically extract solar illumination/shadow direction angle by just using the image processing techniques. The solar illumination angle is an important information in supplementary metadata, of which the availability can improve the feature-based methods. In this work, the shadow area is analyzed in the VHR images in order to propose a new automatic method to determine the shadow direction/solar illumination angle. To this end, the inherent shadow features are involved in the proposed method, and a robust feature is provided.

The shadow applications are reviewed in the next section in order to investigate the application of solar illumination angle information. The proposed method is presented in the third section. Finally, the fourth and fifth sections are devoted to the evaluation and conclusion, respectively.

2. Related Works

Shadow is the clue of the existing tall objects in the studied area. For instance, the shadow information is used to distinguish the buildings from the non-building areas such as roads and parking lots in the urban areas [13]. In this regard, Femiani *et al*. [14] have fused the shadow information and light direction in order to define a structural element to construct the initial segmentation seeds and extract the individual buildings. In another work, Kakooei and Baleghi [10] have used the shadow information and the Gray Level Cooccurrence Matrix (GLCM) features to extract the building map from the pre-disaster vertical image.

There are various feature-based methods for shadow detection. For example, Femiani *et al*. [14] have deployed a simple method to detect shadow areas, which is based on the thresholding of the Y band in the YUV color space. In another work, Mostafa and Abdelhafiz [15] have defined a shadow index by mixing red, green, and blue bands with the principle component analysis. Moreover, Huang and Zhang [16] have proposed a Morphological Shadow Index (MSI) by deploying the spectral and structural shadow features. Recently, Kakooei and Baleghi [1] have proposed a spectral-spatial shadow index and a histogram-based thresholding to extract shadow map in VHR images.

The model-based methods use supplementary metadata such as solar azimuth, which is available in many remote sensing platforms such as the GeoEye-1, QuickBird, and IKONOS-2 satellites [17]. Ok [18] has proposed an automatic two-level graph theory to detect the buildings using shadow information in GeoEye-1 images with a 0.5 m resolution. Moreover, Huang *et al*. [19] have proposed a building detection method using the GaoFen-2 satellites, shadow information, and illumination direction. To this end, the spectral features were mixed with the spatial features including morphological attribute profiles and local binary patterns [19]. Finally, Manno-Kovács and Ok [20] have deployed the shadow information, along with the supplementary metadata file with solar azimuth, solar elevation, and viewing geometry information to detect buildings in the QuickBird and IKONOS-2 datasets.

When shadow direction is not available in RS metadata, it can be determined through the spectral and spatial features. For instance, Sirmacek and Unsalan [21] have used the geometrical center of shadow and its adjacent rooftop in order to calculate the solar illumination direction. In this regard, shadow direction was supposed to be the line connecting the center of a rooftop to the center of its shadow. In another work, Ngo *et al*. [22] have proposed a building rooftop detection method based on the shadow information. They manually determined the illumination angle using a line connecting a corner of a rooftop and its corresponding corner in the shadow area. Therefore, the shadow direction was the ratio between the number of horizontal and vertical pixels of the line.

2.1. Motivation

The shadow direction information is not available in many RS platforms, especially airborne and UAVs. On the other hand, this information can facilitate the object classification methods in urban areas such as building detection [10, 18, 23-26], tree detection [27-29], facade detection [9], and road extraction [30, 31]. Furthermore, there is no automatic method to determine the solar illumination angle, and the manual methods are not applicable in the real-world applications.

The motivation of this paper is to propose a reliable feature, Shadow Low Gradient Direction

(SLGD), to automatically determine shadow and solar illumination direction in the VHR data. The proposed feature is based on the inherent spatial feature of fine-resolution shadow areas.

3. Dataset

The accuracy and the level of details in the shadow detection methods are highly related to the image resolution. The finer resolution of the RS image provides the more detailed structure in the shadow area. Figure 1 shows three images with different resolutions. Figure 1(a) shows the WorldView-3 image of Madrid, Spain with a 1.5 m resolution, in which the shadow area is typically dark with no underlying information. Figure 1(b) shows a 50 cm-resolution image of San Francisco, provided by Digital Globe, in which the shadow area contains more information compared to Figure 1(a). Furthermore, Figure 1(c) shows a 30 cm-resolution image of Chicago, in which the underlying texture of the shadow area is apparently distinguishable. Furthermore, Figure 1(c) shows a sample image with detailed shadow area that was deployed in this study.

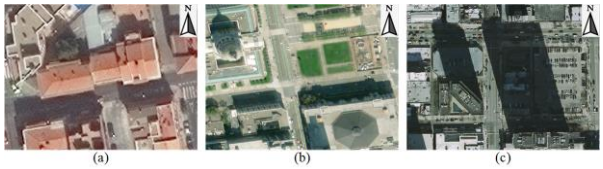

Figure 1. Remote sensing images with different resolutions. (a) WorldView-3 image of Madrid, Spain, with 1.5 m resolution. Free access provided by Digital Globe. (b) Image of San Francisco with 0.5 m resolution. Free access provided by Digital Globe in building footprints project. (c) Image of Chicago with 0.3 m resolution in Inria dataset.

In this work, two datasets are used for evaluation, which are Inria dataset and Google Earth images. The Inria dataset with 0.3 m ground sampling distance contains aerial images that covers 810 km^2 including the train and test data for building detection application. We deployed Chicago (USA) and Vienna (Austria) from the train dataset for evaluation. Each city comprises 36 tiles, and each tile size is 5000 ×5 000 pixels [32]. Furthermore, in this work, we used the Google Earth VHR images in a part of Virginia Beach.

The method is implemented on the Google Earth Engine (GEE) cloud computing platform [33]. GEE is free, and provides various processing tools and datasets [34]. It facilitates the geodata processing at reginal [35, 36], national [37], and global scale [38].

4. Proposed Method

The proposed method is based on the investigation of the spatial darkness intensity of shadow areas in the VHR images. This method can automatically find the solar illumination direction without any additional metadata. To this end, this section is divided into two sub-sections. In the first sub-section, the shadow area is analyzed in the VHR images. Then the proposed Shadow Low Gradient Direction (SLGD) feature is detailed in the second sub-section.

4.1. Shadow Analysis in VHR Images

The shadow darkness intensity is not constant all over the shadow area. Shadow is darker at the bottom of the object than its edges, where it becomes soft and fuzzy. In other words, the darkness intensity decreases in moving from the center to the edges [39]. Figure 2 shows two scenes of the Vienna and Chicago cities in the Inria dataset, in which four factors that affect the intensity of the shadow areas are investigated.

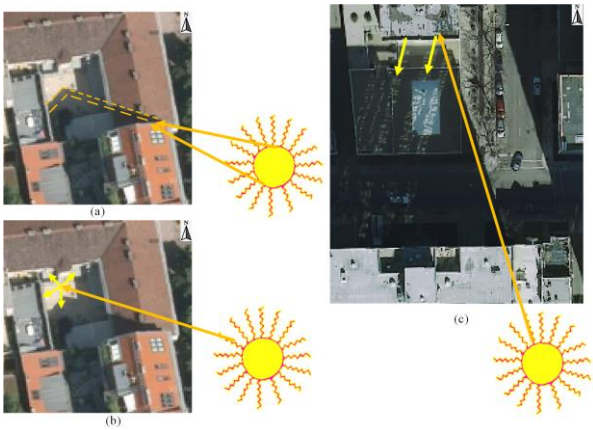

Figure 2. Different factors that affect darkness intensity of shadow. (a) Penumbra effect in Vienna image. (b) Diffuse radiation reflection in Vienna image. (c) Adjacent facade and window reflection in Chicago.

- Underlying structure: Light reflection factor varies according to the material of the underlying structure. Figure 2 shows the shadow areas over different ground surfaces, which apparently differ in brightness intensities.
- Penumbra: Figure 2(a) shows the concept of the penumbra, which means the shadow area is partly blocked by an obstacle [40]. Penumbra causes the shadow to become brighter in moving to the edges.
- Wave behavior of light: Light has two different behaviors in physics including particle behavior and wave behavior [41]. Figure 2(b) shows that the light reflection is diffuse (not specular) according to the wave

behavior [42, 43]. Therefore, in moving from the center of the shadow to its edge, this factor causes a brighter shadow area.

- Opposite facade or wall: Opposite wall or building facade can reflect the sunlight into the shadow area, especially in the urban area. Figure 2(c) shows the reflection light from the facade with many windows. This factor also decreases the darkness intensity in moving to the shadow edges.

All the above-mentioned factors are informative in the shadow area, except the underlying material in which there is no inherent shadow information in moving from one material to another. In order to ignore the material intensity differences in spatial analysis, the high gradient magnitude areas are ignored.

Penumbra, wave behavior of the light, and the opposite facade/wall factors agree that the darkness changes in moving towards the shadow edges contain an interpretable information. Therefore, the shadow intensity decreases in moving from the bottom of the shadow to its edge. Figure 3 shows several spectral profiles of the shadow areas in different directions. The value of the blue band in the shadow area is higher than the other bands. This fact is observable in all shadow profiles in Figure 3, which is considered in the next sub-section for the proposed method. This behavior is also verified by the previous methods [1, 15, 44-47], in which the blue band is considered as the numerator of the proposed shadow indices.

Figure 3(a) shows the shadow area over a homogenous texture in Chicago. Two orthogonal profiles are plotted in Figures 3(d) and 3(e). Figure 3(d) shows an ascending trend from the bottom of the shadow to its edges in profile 1. Considering the transect line of profile 2 in Figure 3(e) is from a shadow edge to another; it does not show a meaningful trend. For Chicago (profile 3) and Vienna (profile 5), the profile lines in RGB bands are shown in Figures 3(b) and 3(c). From the bottom to the edges of shadow, the profiles are shown in Figures 3(f) and 3(h) for Chicago and Vienna, respectively. They also present an ascending trend, like Figure 3(d).

It can be concluded that the high variations are related to the differences of the underlying texture that should be ignored in the proposed method. Figures 3(g) and 3(i) show the information-less transect profile 4 and profile 6 of Chicago and Vienna in RGB bands.

To sum up, the profile analysis of the RGB bands in Figure 3 confirms the shadow darkness behavior in moving from the bottom of the shadow to its edge, which is informative to determine the sunlight illumination direction.

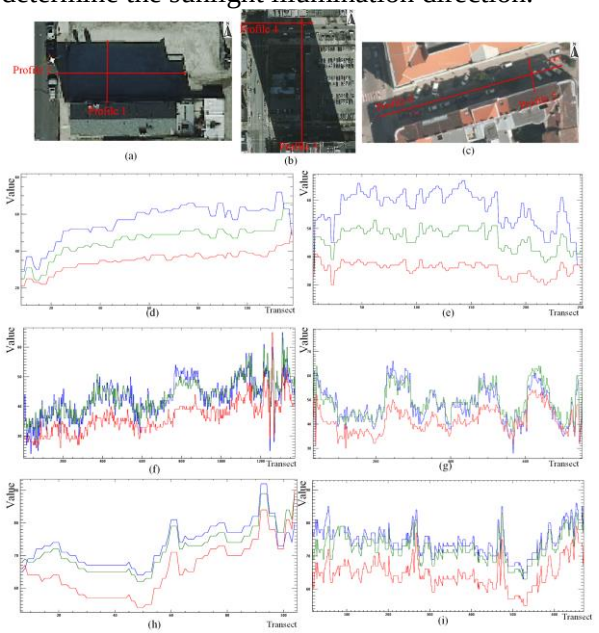

Figure 3. Shadow profiles in RGB images of (a, b) Chicago, and (c) Vienna. (d-i) Profiles in Red-Green-Blue color space. (d) Profile 1. (e) Profile 2. (f) Profile 3. (g) Profile 4. (h) Profile 5. (i) Profile 6.

4.2. Shadow Low Gradient Direction (SLGD) Feature

The framework of the proposed method to find the shadow/illumination direction is shown in Figure 4. An RGB VHR image is the only input of the system, and the output of the system is the shadow/illumination direction angle.

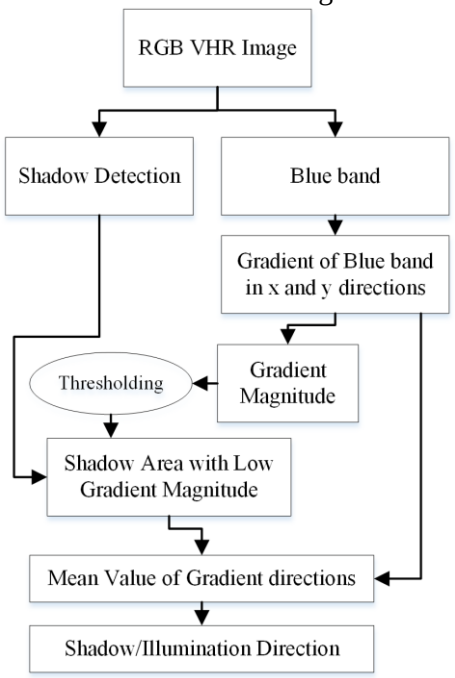

Figure 4. Framework of the proposed method to find shadow/illumination direction. VHR RGB image is the only input and direction is the output.

A feature-based shadow detection method is required to highlight the shadow areas. We deployed the method proposed by Kakooei and Baleghi [1] that is based on the spectral and spatial operations. They proposed a Spectral-Spatial Shadow Index (SSSI) based on the RGB bands, Principle Component Analysis (PCA), and a GLCM feature. SSSI is shown in Equation 1.

$$SSSI = \frac{PC_1 + B + SENT}{R + G + 1} \quad (1)$$

where R, G, and B are the red, green, and blue bands, respectively. PC_1 is the band corresponding to the largest Eigen value of PCA and SENT is the sum of entropy derived from the GLCM analysis. The SSSI index is thresholded according to the histogram information to generate the binary shadow map *shd* [1].

In our method, the shadow direction analysis is based on the blue band, which has a relatively high value in the shadow area and its importance was discussed in the previous sub-section. The gradient of the blue band was considered for the spatial analysis.

The gradient of the blue band in the *x* and *y* directions, named *Px* and *Py*, are calculated in Equations 2, and 3.

$$Px = \frac{d\ Blue}{d\ x} \quad (2)$$

$$Py = \frac{d\ Blue}{d\ y} \quad (3)$$

Afterward, the magnitude *mag* of the blue band gradient is calculated in Equation 4.

$$Mag = \sqrt{Py^2 + Px^2} \quad (4)$$

It can be concluded that the large gradient values are related to the underlying material, and are not related to the shadow direction. Therefore, this is a critical step in the proposed method to ignore the areas with a large gradient magnitude and decide according to the areas with a low gradient magnitude.

In this method, the threshold value of the gradient magnitude is empirically set to 5 in an 8-bit unsigned integer data, ranging from 0 to 255. To this end, the shadow profiles in Figure 3 were investigated and their backgrounds' materials were considered. In other words, it was found that moving from one pixel to a neighbourhood pixel on the same material did not change the gradient magnitude more than 5.

Therefore, the region of interest ROI is limited to the low gradient magnitude areas according to Equation 5.

$$ROI = \begin{cases} 1 & IF\ shd = 1\ and\ Mag < 5 \\ 0 & O.W. \end{cases} \quad (5)$$

Then the mean values of *Px* and *Py*, named *mPx* and *mPy*, are found in e ROI according to Equations 6 and 7.

$$mPx = \frac{1}{N}\sum_{ROI(i,j)=1} Px(i,j) \quad (6)$$

$$mPy = \frac{1}{N}\sum_{ROI(i,j)=1} Py(i,j) \quad (7)$$

where *N* is the total number of true pixels in the ROI, and the indices *i* and *j* show the position of the *Px* and *Py* pixels in ROI. Finally, the angle θ between *mPy* and *mPx* was calculated via Equation 8 as the shadow direction.

$$\theta = \tan^{-1}\left(\frac{mPy}{mPx}\right) \times \frac{180}{\pi} \quad (8)$$

where tan^{-1} finds the angle between *mPy* and *mPx* in radians. Then angle θ was converted to degree by a constant multiplier $\frac{180}{\pi}$, and was refined by the conditional statement in Equation 9. Finally, the refined value indicates the proposed SLGD index, which can automatically determine the shadow and solar illumination direction in the RGB VHR images.

$$SLGD = \begin{cases} \theta - 180 & IF\ \theta > 0\ and\ mPy < 0 \\ \theta + 180 & IF\ \theta < 0\ and\ mPy > 0 \\ 0 & O.W. \end{cases} \quad (9)$$

5. Evaluation

In the previous studies, the solar illumination angle was either in the metadata or determined manually, and thus there is no automatic method for comparison. We designed two different strategies in order to evaluate the proposed method. Firstly, we compared the proposed automatic shadow direction with the manual shadow direction deployed by Ngo *et al*. [22], which was based on the line connecting one corner of a building to the corresponding corner in the shadow area. This verifies the reliability of the proposed automatic procedure. Secondly, we utilized the proposed shadow direction in order to refine the shadow map proposed by Kakooei and Baleghi [1]. To this end, the shadow segments [1] that did no align with the proposed automatic shadow direction were removed from the shadow map. Therefore, this work was evaluated in a real application.

5.1. Automatic *vs.* Manual Shadow Direction

Figure 5 shows eight scenes of Chicago, Vienna, and Virginia Beach. It shows the shortcomings of the Ngo *et al*. [22] method in the manual shadow

direction determination, especially for the stand-alone buildings.

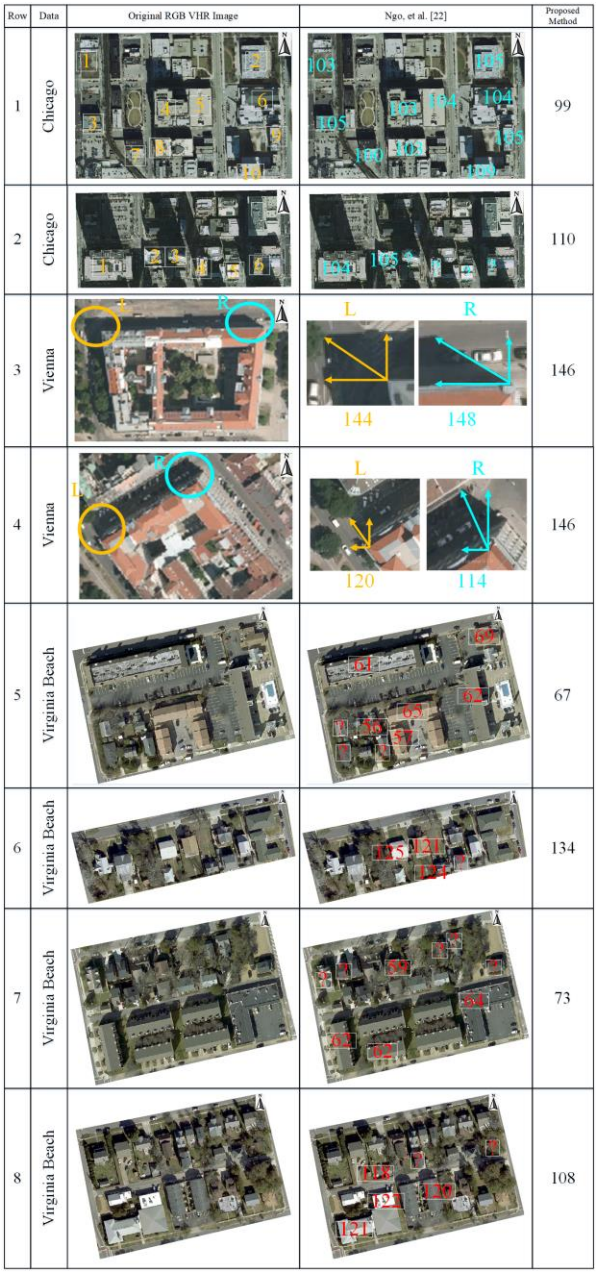

Figure 5. Comparing determination of shadow direction angle. First Column indicates the row number. Second column shows the image location. Third column shows the original RGB VHR images. Shadow directions determined manually by Ngo *et al.* [22] are labeled in the fourth column. Last column shows the result of our proposed method.

The first row of Figure 5 shows a part of Chicago in which several shadow directions are determined manually and labeled in the fourth column. Our proposed method automatically determines the shadow direction angle to be 99 degrees. The second row shows another part of the Chicago image. The manual method by Ngo *et al*. [22] could find the shadow direction in the buildings 1 and 2 but the mixture of different object shadows in the buildings 3-6 made the manual labeling impossible. In addition, some shadow areas are not reliable as they are affected by an adjacent object. For instance, the shadow area is formed on the adjacent low-rise building instead of being formed on the ground. Therefore, the shadow directions of the buildings numbers 3-6 could not be determined manually. On the other hand, our proposed method finds the shadow direction angle to be 110 degrees.

The third and the fourth rows of Figure 5 show two scenes of Vienna, in which our proposed method finds the shadow direction to be 146. In the third row, the shadow direction of a building is determined manually according to two different corners of a building. Therefore, the manual shadow direction determination according to the left and right corners results is 144 and 148, respectively. Considering that the procedure is manual, even one faulty pixel could result in different values.

The manual shadow direction determination by Ngo *et al*. [22] assumes that the input image is a vertical orthophoto without facade information. Therefore, if the building facade is visible like in the fourth row of Figure 5, the manual shadow direction determination does not provide a reasonable result. On the other hand, our proposed method just considers the shadow inherent darkness variation, and is not dependant on the imagery angle.

For more investigation and in order to verify the performance of the proposed method, four scenes of Virginia Beach are shown in the rows 5 to 8. In addition to the adjacent building that misleads the manual interpretation, these areas are covered by many trees that effect the manual analysis. On the other hand, the proposed method can handle the scene, and determine the shadow direction automatically.

5.2. Shadow Direction in a Real Application

We used five factors in order to evaluate the effect of the proposed shadow direction on refining the shadow map proposed by Kakooei and Baleghi [1]. Then we compared the shadow detection accuracy against the Huang and Zhang [16], Femiani *et al*. [14], Mostafa and Abdelhafiz [15], and Kakooei and Baleghi [1] methods.

These factors are Producer Accuracy (PA), User Accuracy (UA), Overall Accuracy (OA), F1 Score, and Kappa (K) coefficient. Supposing that TP is the number of shadow pixels that are truly detected as shadow, TN is the number of non-shadow pixels that are truly detected as non-

shadow, FP is the number of non-shadow pixels that are falsely detected as shadow, and FN is the number of shadow pixels that are falsely detected as non-shadow; the evaluation factors are defined as follow:

$$PA = \frac{TP}{TP + FP} \quad (10)$$

$$UA = \frac{TP}{TP + FN} \quad (11)$$

$$OA = \frac{TP + TN}{TP + TN + FP + FN} \quad (12)$$

$$F1 = 2\frac{PA \times UA}{PA + UA} \quad (13)$$

Table 1 summarizes the comparison in different studied areas. As the proposed feature is deployed just as a post-processing refinement step, it shows a little UA reduction in all the studied areas. This is due to the potential of removing some TP segments when it tries to decrease FP and remove the non-shadow areas. However, PA shows such a significant improvement that improves the OA, F1 score, and Kappa coefficient values. Therefore, it can be concluded that the proposed method provides a reliable and accurate shadow direction in large-scale analysis.

Table 1. Analytical evaluation of the proposed feature in shadow detection application at Virginia Beach, Chicago, and Vienna.

Area	Assessment	[14]	[15]	[16]	[1]	Proposed
Virginia Beach	PA%	37.99	85.05	54.76	85.20	90.43
	UA%	97.81	60.47	96.40	95.95	94.74
	OA%	77.43	74.67	83.01	93.40	95.04
	F1 Score	54.72	70.68	69.84	90.26	92.53
	K	0.4334	0.4948	0.5920	0.8529	0.8883
Chicago	PA%	5.07	91.23	17.45	90.62	93.49
	UA%	87.12	93.08	94.33	98.02	97.55
	OA%	38.31	89.97	46.10	92.77	94.47
	F1 Score	9.58	91.5	29.45	95.32	95.48
	K	0.0268	0.7829	0.1167	0.8469	0.8838
Vienna	PA%	0.11	97.13	45.98	91.37	95.29
	UA%	96.00	89.48	99.49	98.19	97.66
	OA%	52.45	93.19	74.18	95.09	96.83
	F1 Score	0.22	93.15	62.89	94.66	96.46
	K	0.0011	0.8642	0.4693	0.9013	0.936

6. Conclusion

The shadow direction is an informative feature in the optical RS applications. It facilitates the shadow-based procedure such as object height estimation. Furthermore, its role in the urban area analysis is undeniable. Therefore, we proposed a new feature in order to design an automatic shadow direction determination method and facilitate the real-world applications.

The proposed feature SLGD can automatically find the shadow direction. Two improvements were highlighted in the proposed method. Firstly, the manual methods were pixel-based, and were limited to the vertical imagery, while the proposed method considers the spatial behavior of the shadow darkness, and does not limit the imagery angle. Secondly, the previous methods could hardly be deployed in dense urban areas, while the proposed method could handle a batch of shadow regions in dense areas.

The proposed method is based on the inherent spatial variation of shadow darkness intensity. This is also along with the physical behavior of light. Therefore, the underlying material variation is ignored through the gradient magnitude information. Also the gradient direction in the low gradient magnitude areas is considered to calculate SLGD.

The proposed method was evaluated on the VHR images of Chicago, Virginia Beach, and Vienna. Finally, in order to evaluate the performance of the proposed automatic method, it was compared against a manual method.

Acknowledgment

The authors acknowledge the funding support of the Iran National Science Foundation (INSF) through the Grant program No. 99022825.

References

[1] M. Kakooei and Y. Baleghi, "Shadow detection in very high resolution RGB images using a special thresholding on a new spectral–spatial index," *Journal of Applied Remote Sensing*, Vol. 14, No. 1, p. 016503, 2020.

[2] M. Kakooei and Y. Baleghi, "Fusion of satellite, aircraft, and UAV data for automatic disaster damage assessment," *International journal of remote sensing*, Vol. 38, No. 8-10, pp. 2511-2534, 2017.

[3] M. Kakooei and Y. Baleghi, "Spectral Unmixing of Time Series Data to Provide Initial Object Seeds for Change Detection on Google Earth Engine," in *2019 27th Iranian Conference on Electrical Engineering (ICEE)*, 2019, pp. 1402-1407: IEEE.

[4] Y. Mostafa, "A review on various shadow detection and compensation techniques in remote sensing images," *Canadian Journal of Remote Sensing*, Vol. 43, No. 6, pp. 545-562, 2017.

[5] G. Vijayan, S. Reshma, F. Dhanya, S. Anju, G. R. Nair, and R. Aneesh, "A novel shadow removal algorithm using Niblack segmentation in satellite images," in *Communication Systems and Networks (ComNet), International Conference on*, 2016, pp. 184-189: IEEE.

[6] M. Kakooei and Y. Baleghi, "VHR Semantic Labeling by Random Forest Classification and Fusion of Spectral and Spatial Features on Google Earth Engine," *Journal of AI and Data Mining*, 2020.

[7] I. Doustfatemeh and Y. Baleghi, "Comprehensive urban area extraction from multispectral medium spatial resolution remote-sensing imagery based on a novel structural feature," *International Journal of Remote Sensing*, Vol. 37, No. 18, pp. 4225-4242, 2016.

[8] N. Kadhim, M. Mourshed, and M. Bray, "Shadow detection from very high resoluton satellite image using grabcut segmentation and ratio-band algorithms," 2015: International Society for Photogrammetry and Remote Sensing.

[9] M. Kakooei, Y. Baleghi, and M. Amani, "Adaptive thresholding for detecting building facades with or without openings in single-view oblique remote sensing images," *Journal of Applied Remote Sensing*, Vol. 15, No. 3, p. 036511, 2021.

[10] M. Kakooei and Y. Baleghi, "A two-level fusion for building irregularity detection in post-disaster VHR oblique images," *Earth Science Informatics*, pp. 1-19, 2020.

[11] Y. Li, P. Gong, and T. Sasagawa, "Integrated shadow removal based on photogrammetry and image analysis," *International Journal of Remote Sensing*, Vol. 26, No. 18, pp. 3911-3929, 2005.

[12] W. Huang and M. Bu, "Detecting shadows in high-resolution remote-sensing images of urban areas using spectral and spatial features," *International Journal of Remote Sensing*, Vol. 36, No. 24, pp. 6224-6244, 2015.

[13] E. Li, J. Femiani, S. Xu, X. Zhang, and P. Wonka, "Robust rooftop extraction from visible band images using higher order CRF," *IEEE Transactions on Geoscience and Remote Sensing*, Vol. 53, No. 8, pp. 4483-4495, 2015.

[14] J. Femiani, E. Li, A. Razdan, and P. Wonka, "Shadow-based rooftop segmentation in visible band images," *IEEE Journal of Selected Topics in Applied Earth Observations and Remote Sensing*, vol. 8, No. 5, pp. 2063-2077, 2015.

[15] Y. Mostafa and A. Abdelhafiz, "Accurate shadow detection from high-resolution satellite images," *IEEE Geoscience and Remote Sensing Letters*, Vol. 14, No. 4, pp. 494-498, 2017.

[16] X. Huang and L. Zhang, "Morphological building/shadow index for building extraction from high-resolution imagery over urban areas," *IEEE Journal of Selected Topics in Applied Earth Observations and Remote Sensing*, Vol. 5, No. 1, pp. 161-172, 2012.

[17] C. Senaras and F. T. Y. Vural, "A self-supervised decision fusion framework for building detection," *IEEE Journal of Selected Topics in Applied Earth Observations and Remote Sensing*, Vol. 9, No. 5, pp. 1780-1791, 2016.

[18] A. O. Ok, "Automated detection of buildings from single VHR multispectral images using shadow information and graph cuts," *ISPRS journal of photogrammetry and remote sensing*, Vol. 86, pp. 21-40, 2013.

[19] H. Huang, G. Sun, J. Rong, A. Zhang, and P. Ma, "Multi-feature Combined for Building Shadow detection in GF-2 Images," in *2018 Fifth International Workshop on Earth Observation and Remote Sensing Applications (EORSA)*, 2018, pp. 1-4: IEEE.

[20] A. Manno-Kovács and A. O. Ok, "Building detection from monocular VHR images by integrated urban area knowledge," *IEEE Geoscience and Remote Sensing Letters*, Vol. 12, No. 10, pp. 2140-2144, 2015.

[21] B. Sirmacek and C. Unsalan, "Building detection from aerial images using invariant color features and shadow information," in *Computer and Information Sciences, 2008. ISCIS'08. 23rd International Symposium on*, 2008, pp. 1-5: IEEE.

[22] T.-T. Ngo, V. Mazet, C. Collet, and P. De Fraipont, "Shape-Based Building Detection in Visible Band Images Using Shadow Information," *IEEE Journal of Selected Topics in Applied Earth Observations and Remote Sensing*, Vol. 10, No. 3, pp. 920-932, 2017.

[23] A. O. Ok, C. Senaras, and B. Yuksel, "Automated detection of arbitrarily shaped buildings in complex environments from monocular VHR optical satellite imagery," *IEEE Transactions on Geoscience and Remote Sensing*, Vol. 51, No. 3, pp. 1701-1717, 2013.

[24] S. Xu *et al.*, "Automatic Building Rooftop Extraction from Aerial Images via Hierarchical RGB-D Priors," *IEEE Transactions on Geoscience and Remote Sensing*, No. 99, pp. 1-19, 2018.

[25] S. Li, H. Tang, X. Huang, T. Mao, and X. Niu, "Automated Detection of Buildings from Heterogeneous VHR Satellite Images for Rapid Response to Natural Disasters," *Remote Sensing*, Vol. 9, No. 11, p. 1177, 2017.

[26] A. Rahimzadeganasl and E. Sertel, "Automatic building detection based on CIE LUV color space using very high resolution pleiades images," in *Signal Processing and Communications Applications Conference (SIU), 2017 25th*, 2017, pp. 1-4: IEEE.

[27] S. Basu *et al.*, "A semiautomated probabilistic framework for tree-cover delineation from 1-m NAIP imagery using a high-performance computing architecture," *IEEE Transactions on Geoscience and Remote Sensing*, Vol. 53, No. 10, pp. 5690-5708, 2015.

[28] A. Ozdarici-Ok, "Automatic detection and delineation of citrus trees from VHR satellite imagery," *International Journal of Remote Sensing*, Vol. 36, No. 17, pp. 4275-4296, 2015.

[29] M. Kakooei and Y. Baleghi, "Leaf-Less-Tree feature for semantic labeling applications on Google Earth Engine," in *Telecommunications (IST), 2018 9th International Symposium on*, 2018: IEEE.

[30] G. Cheng, Y. Wang, S. Xu, H. Wang, S. Xiang, and C. Pan, "Automatic Road Detection and Centerline Extraction via Cascaded End-to-End Convolutional Neural Network," *IEEE Transactions on Geoscience and Remote Sensing*, Vol. 55, No. 6, pp. 3322-3337, 2017.

[31] Y. Bae, W.-H. Lee, Y. Choi, Y. W. Jeon, and J. B. Ra, "Automatic road extraction from remote sensing images based on a normalized second derivative map," *IEEE Geoscience and remote sensing letters*, Vol. 12, No. 9, pp. 1858-1862, 2015.

[32] E. Maggiori, Y. Tarabalka, G. Charpiat, and P. Alliez, "Can semantic labeling methods generalize to any city? the inria aerial image labeling benchmark," in *IEEE International Symposium on Geoscience and Remote Sensing (IGARSS)*, 2017.

[33] N. Gorelick, M. Hancher, M. Dixon, S. Ilyushchenko, D. Thau, and R. Moore, "Google Earth Engine: Planetary-scale geospatial analysis for everyone," *Remote Sensing of Environment*, Vol. 202, pp. 18-27, 2017.

[34] M. Amani *et al.*, "Google Earth Engine Cloud Computing Platform for Remote Sensing Big Data Applications: A Comprehensive Review," *IEEE Journal of Selected Topics in Applied Earth Observations and Remote Sensing*, 2020.

[35] M. Amani *et al.*, "Application of Google Earth Engine Cloud Computing Platform, Sentinel Imagery, and Neural Networks for Crop Mapping in Canada," *Remote Sensing*, Vol. 12, No. 21, p. 3561, 2020.

[36] M. Amani *et al.*, "Evaluation of the Landsat-based Canadian Wetland Inventory Map using Multiple Sources: Challenges of Large-scale Wetland Classification using Remote Sensing," *IEEE Journal of Selected Topics in Applied Earth Observations and Remote Sensing*, 2020.

[37] A. Ghorbanian, M. Kakooei, M. Amani, S. Mahdavi, A. Mohammadzadeh, and M. Hasanlou, "Improved land cover map of Iran using Sentinel imagery within Google Earth Engine and a novel automatic workflow for land cover classification using migrated training samples," *ISPRS Journal of Photogrammetry and Remote Sensing*, Vol. 167, pp. 276-288, 2020.

[38] M. Kakooei, A. Nascetti, and Y. Ban, "Sentinel-1 global coverage foreshortening mask extraction: An open source implementation based on Google Earth Engine," in *IGARSS 2018-2018 IEEE International Geoscience and Remote Sensing Symposium*, 2018, pp. 6836-6839: IEEE.

[39] M. Minnaert, *The nature of light and colour in the open air*. Courier Corporation, 2013.

[40] N. Su, Y. Zhang, S. Tian, Y. Yan, and X. Miao, "Shadow detection and removal for occluded object information recovery in urban high-resolution panchromatic satellite images," *IEEE Journal of Selected Topics in Applied Earth Observations and Remote Sensing*, Vol. 9, No. 6, pp. 2568-2582, 2016.

[41] C. Meis, *LIGHT AND VACUUM: The Wave-Particle Nature of the Light and the Quantum Vacuum. Electromagnetic Theory and Quantum Electrodynamics Beyond the Standard Model*. World Scientific, 2017.

[42] L. B. Wolff, S. K. Nayar, and M. Oren, "Improved diffuse reflection models for computer vision," *International Journal of Computer Vision*, Vol. 30, No. 1, pp. 55-71, 1998.

[43] W. M. Irvine, "The shadowing effect in diffuse reflection," *Journal of Geophysical Research*, Vol. 71, No. 12, pp. 2931-2937, 1966.

[44] V. Arévalo, J. González, and G. Ambrosio, "Shadow detection in colour high-resolution satellite images," *International Journal of Remote Sensing*, Vol. 29, No. 7, pp. 1945-1963, 2008.

[45] X. Liu, Z. Hou, Z. Shi, Y. Bo, and J. Cheng, "A shadow identification method using vegetation indices derived from hyperspectral data," *International Journal of Remote Sensing*, Vol. 38, No. 19, pp. 5357-5373, 2017.

[46] Y. Mostafa and M. A. Abdelwahab, "Corresponding regions for shadow restoration in satellite high-resolution images," *International Journal of Remote Sensing*, pp. 1-15, 2018.

[47] N. Tatar, M. Saadatseresht, H. Arefi, and A. Hadavand, "a New Object-Based Framework to Detect Shodows in High-Resolution Satellite Imagery Over Urban Areas," *The International Archives of Photogrammetry, Remote Sensing and Spatial Information Sciences*, Vol. 40, No. 1, p. 713, 2015.

تعیین خودکار جهت سایه با استفاده از ویژگی جهت گرادیان های کوچک سایه در تصاویر RGB سنجش از دور با رزولوشن خیلی بالا

محمد کاکوئی و یاسر بالغی*

دانشگاه صنعتی نوشیروانی بابل، دانشکده مهندسی برق و کامپیوتر، خیابان شریعتی، بابل، ایران.

ارسال ۲۰۲۱/۱/۱۰؛ بازنگری ۲۰۲۱/۰۹/۰۵؛ پذیرش ۲۰۲۱/۱۲/۲۲

چکیده:

تشخیص سایه دارای اطلاعات ارزشمندی در کاربردهای مختلف سنجش از دور است که از این جمله میتوان بـه تخمـین ارتفـاع سـاختمان اشـاره کـرد. مناطق سایه در جهت مقابل تابش نور خورشید به اشیای بلند ایجاد میشود و در نتیجه، برای پیدا کردن مناطق محتمل تشکیل سایه، به اطلاعـات زاویـه تابش نور خورشید نیاز است. در سالیان اخیر، استفاده از تصاویر با رزولوشن خیلی بالا (VHR) موجـب شـده کـه جزییـات بیشـتری از منـاطق سـایه در دسترس باشد. از این روی، انگیزه‌ی این مقاله پیشنهاد ویژگی قابل اعتمادی به نام جهت گرادیان های کوچک سـایه (SLGD) اسـت کـه مـی‌توانـد بـه صورت خودکار جهت سایه و تابش نور خورشید را در تصاویر VHR تعیین کند. ویژگی پیشنهادی براساس مشخصات مکانی ذاتی سـایه در منـاطقی بـا رزولوشن بالا است. در نتیجه، می توان کاربردهای مبتنی بر سایه را خصوصا زمانی که اطلاعات تابش خورشید در دسترس نباشـد، تسـهیل کـرد. شـدت تاریکی سایه به دو مولفه وابسته است که شامل جنس سطح زیرین و نور بازگشتی خورشید است. نـور بازگشـتی توسـط تحلیـل گرادیـان جهـت دار در مناطق با اندازه گرادیان کوچک بررسی می‌شود. این ویژگی اطلاعات بازتاب خورشید را در نظر می‌گیرد و از اطلاعات جنس زیرین صـرف نظـر مـی‌کنـد. روش پیشنهادی در سامانه محاسبات ابری Google Earth Engine پیاده سازی شده است و از داده VHR با رزولوشن ۰/۳ متـر اسـتفاده شـده اسـت. درنهایت، کارایی SLGD در تعیین جهت سایه و تصحیح نقشه سایه ارزیابی می‌شود.

کلمات کلیدی: جهت سایه، استخراج ویژگی، شناسایی سایه، VHR، Google Earth Engine.